INTL JOURNAL OF ELECTRONICS AND TELECOMMUNICATIONS, 2026, VOL. 72, NO. 3, PP. 1-8
Manuscript received March 13,2026; revised June, 2026. doi: 10.24425/ijet.2026.157945

The influence of bottom slope on sound signals transmission to receiver (Part B) buried in bottom sediments

Roman Salamon, and Jacek Marszal

***Abstract*—Underwater acoustic communications (UAC) in shallow waters is an extremely challenging task. This becomes even more difficult when reliable communications with an object buried in seabed sediments is required. The work presented in two articles (Part A and Part B) is a continuation of the earlier work published in [1]. The articles present the simulation of an acoustic transmission channel, taking into account the bottom slope angle. The simulation utilize the impulse response method and the image source ray tracing technique. The articles present examples of data transmission in a shallow channel with a sloping bottom to a receiver submerged in the water column (Part A) and to a receiver buried in seabed sediments (Part B).**

***Keywords*—underwater acoustic communications; UAC; shallow water channel; multipath propagation; bottom slope**

I. Introduction

THE Department of Signals and Systems at the Faculty of Electronics, Telecommunications, and Informatics of the Gdańsk University of Technology has been conducting research on underwater wireless communication in shallow waters for many years. This work includes theoretical analyses [1] and tests and measurements in actual field conditions [2-6]. The previous article [1] presented an analysis of acoustic wave propagation conditions in shallow water between a transmitter immersed in the water column and a receiver placed in the water column or buried in bottom sediments. For simplicity, the analysis assumed a constant water depth. In these articles (part A and part B), the presented analysis takes into account the slope of the bottom - rising or falling. In part A, the analysis concerns the transmission of acoustic signals to a receiver placed in the water column, and in part B, to a receiver buried in bottom sediments. Similar to article [1], the analysis was conducted using the image source method [7-10] and the impulse response method. This approach to analysing acoustic signal propagation in shallow waters differs from that typically presented in the literature, e.g. [11-13]. The use of the impulse response method allows for the analysis of any type of signal and any transmission conditions.

The paper was written as a result of the research project No. DOB-SZAFIR/01/B/017/04/2021 financed by The National Centre for Research and Development of the Republic of Poland.

Authors are with Gdansk University of Technology, Faculty of Electronics, Telecommunications and Informatics, Department of Signals and Systems, Gdańsk, Poland. (e-mail: jacek.marszal@pg.edu.pl).

II. Sound Wave Paths

Sound waves emitted in water by a transmitter submerged at a depth h reach a receiver buried in the bottom sediments at a depth g and located at a distance z from the transmitter. The flat bottom is inclined at an angle β to the water surface. Fig. 1 shows the sound wave path after three reflections, with the first reflection returning from the water surface. The x-coordinates of the reflection points are denoted as x_{nk}, where n is the number of reflections and k is the number of the consecutive reflection. Similarly, the y-coordinates of the reflection points are denoted as y_{nk}. The x-coordinate of the wave path in the bottom sediments is denoted x_{nko}. There is only one path satisfying the condition of equality of the angle of incidence to the angle of reflection and the angle of refraction δ_n satisfying Snell's law of refraction. Such a path is determined by the first angle of incidence α_n on the water surface.

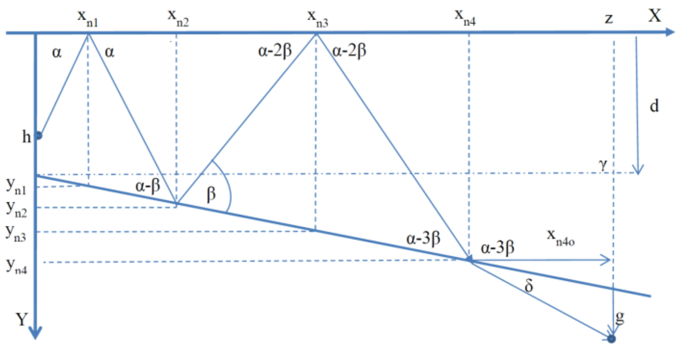

Fig. 1. Sound wave path when reflected first from the water surface.

From the geometric relationships seen in the Fig. 1, the coordinates x_{nk} can be determined using the Eq. (1-8):

$$x_{n1} = \frac{h}{tg\alpha_n} \tag{1}$$

odd k:

$$x_{nk} = \frac{d + x_{n(k-1)}\{tg[\alpha_n - (k-1)\beta] + tg\beta\}}{tg[\alpha_n - (k-1)\beta]}$$

$$k = 2, \dots n \tag{2}$$

$$y_{nk} = 0 \tag{3}$$

even k:

$$x_{nk} = \frac{d + x_{n(k-1)} tg[\alpha_n - (k-2)\beta]\}}{tg[\alpha_n - (k-2)\beta] - tg\beta} \quad k = 2, \dots n \tag{4}$$

$$y_{nk} = d + x_{nk} tg\beta \tag{5}$$

$$\delta_n = \arccos\{\frac{c_d}{c}\cos([\alpha_n - (n-1)\beta]\} \tag{6}$$

$$x_{no} = \frac{g}{tg(\delta_n + \beta) - tg\beta} \tag{7}$$

$$y_{no} = d + g + x_{nko} tg\beta \tag{8}$$

The coordinates *x* satisfy Eq. (9) for the angle sought α_n:

$$x_{nk} + x_{no} = z \tag{9}$$

The Eq. (10) is solved numerically for each considered number of reflections *n* and the assumed channel parameters. By inserting the determined angle α_n into the formulas, all the reflection points from the water surface and the bottom are obtained. These coordinates describe the sound wave paths, examples of which are shown in Fig. 2-3. They were made for the following channel and system parameters: z = 100 m, d = 20 m, h = 5 m, g = 2 m, c = 1,500 m/s, c_d = 1,800 m/s. The bottom slope angles are described in the figure legends.

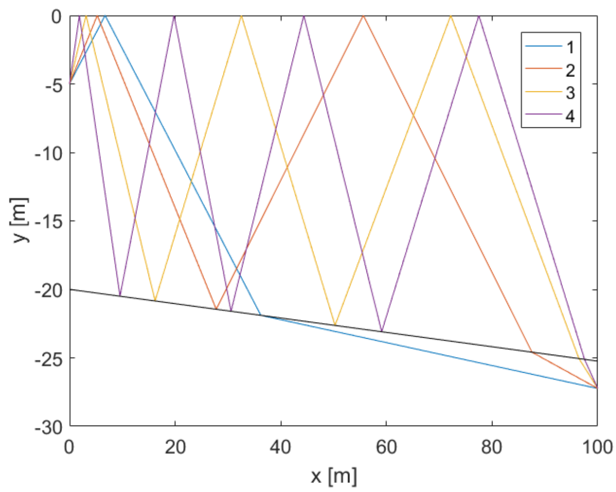

Fig. 2. Sound wave paths at an angle of bottom slope β = 3°.

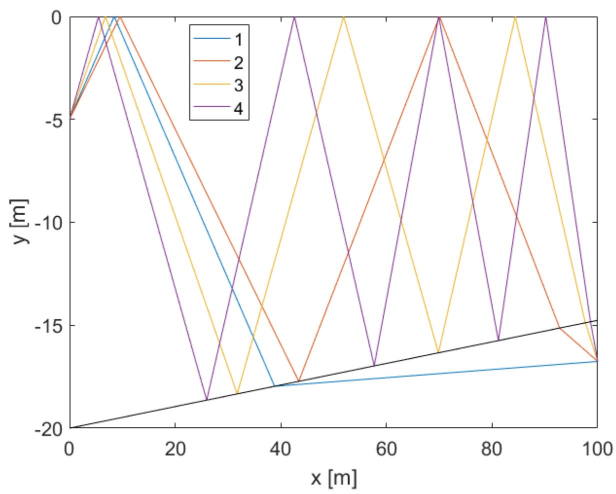

Fig. 3. Sound wave paths at an angle of bottom slope β = −3°.

The sound wave path for three reflections, with the first returning from the bottom, is shown in Fig. 4.

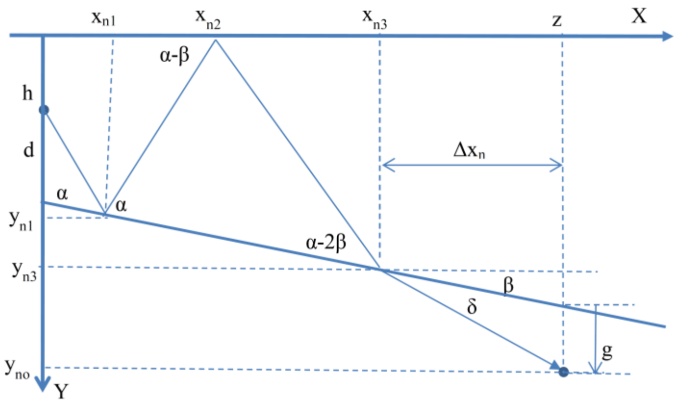

Fig. 4. Sound wave paths when reflected first from the bottom.

The coordinates x_{n1} and y_{n1} have the forms of Eq. (10)

$$x_{n1} = \frac{d-h}{tg(\alpha_n + \beta) - tg\beta}$$

$$y_{n1} = d + x_{n1} tg\beta \tag{10}$$

For odd reflections *k*, the coordinates of the reflection points x_{nk} are described by Eq. (4), and for the others, by Eq. (11-13):

$$y_{n1} = d + x_{n1} tg\beta \tag{11}$$

$$x_{no} = \frac{g}{tg(\delta_n + \beta) - tg\beta} \tag{12}$$

$$y_{no} = d + x tg\beta + g \tag{13}$$

For even reflections *k*, the coordinates x_{nk} and y_{nk} are given by Eq. (2- 3)

The angles α_n are the solutions of Eq. (9), in which the above relationships are used. Once this equation is solved, the coordinates of the reflections are determined from the formulas, and the sound wave paths are determined from these. Fig. 5-6 show example paths for the channel and system parameters for which Fig. 2-3 were made.

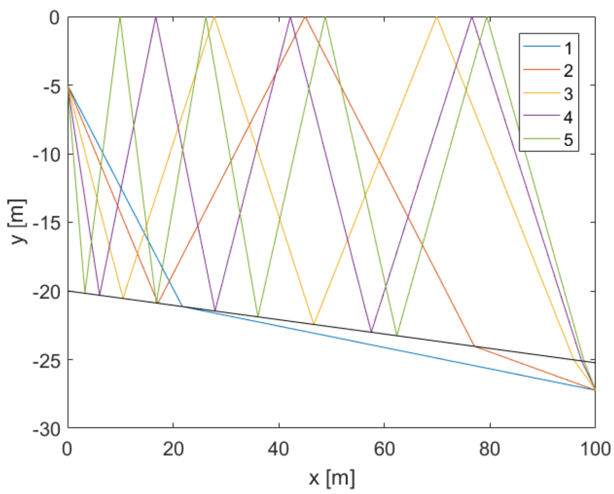

Fig. 5. Sound wave paths at an angle of bottom slope β = 3°.

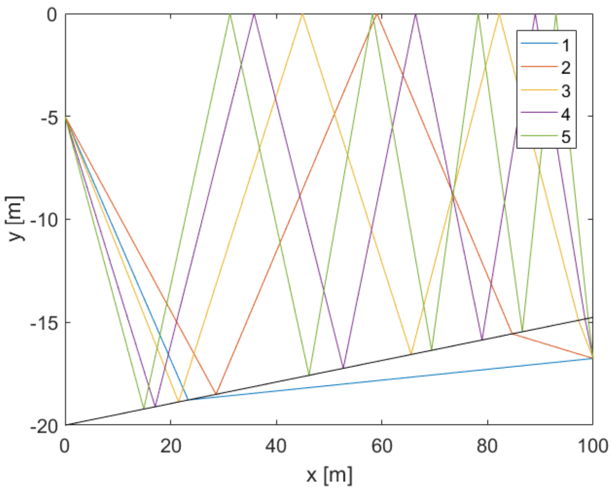

Fig. 6. Sound wave paths at an angle bottom slope $\beta = -3°$.

III. Pulse Responses and Transfer Functions

The pulse responses, which are the signals received for a Dirac pulse input, depend on the path lengths s_n that the pulses travel. These lengths are determined from Eq. (14-15) for propagation in water:

$$r_{nk} = \sqrt{\left(x_{nk} - x_{n,k-1}\right)^2 + \left(y_{nk} - y_{n,k-1}\right)^2}$$

$$n = 2, \ldots, N, k = 1, \ldots, n \quad (14)$$

$$s_n = \sum_{k=1}^{n} r_{nk} \quad (15)$$

and from the Eq. (16) for propagation in the bottom sediments:

$$s_{no} = \sqrt{x_{no}^2 + y_{no}^2} \quad (16)$$

The amplitudes of the received Dirac pulses are described by the Eq. (17):

$$A_n = \frac{s_1}{s_n + s_{no}} 10^{-(\alpha_a s_n + \alpha_b)/20} A \quad (17)$$

where s_1 = 1 m, α_a is the logarithmic absorption attenuation coefficient in water [dB/m], α_b is the logarithmic absorption attenuation coefficient for the bottom sediments, and A is the amplitude of the pressure emitted by the transmitter at a distance s_1 from the surface. In the numerical calculation, A = 1, ignoring its physical magnitude.

At the boundary surfaces, the pulse amplitudes are reduced by the coefficients described by the Eq. (18):

$$R_{nk} = \frac{z_b \sin \alpha_{nk} - z_w \sin\beta_{nk}}{z_b \sin \alpha_{nk} + z_w \sin\beta_{nk}} \quad (18)$$

where $\alpha_{nk} = \alpha_n\text{-}(k\text{-}1)\beta$ are the angle of incidence at the boundary surfaces and β_{nk} are the angle of refraction of the acoustic wave at the boundary between water and bottom sediment. The symbol z_b denotes the characteristic impedance of the bottom sediments, and z_{in} denotes the same for water. A simplified assumption is made that the reflection coefficient at the water/air interface is $R_{nk} = -1$.

The angle β_{nk} is determined from Snell's law by the Eq. (19):

$$\frac{cos\alpha_{nk}}{cos\beta_{nk}} = \frac{c_w}{c_d} \quad (19)$$

where c_w is the sound wave velocity in the water, and c_b is the sound wave velocity within the bottom sediments.

Subsequent pulse responses are delayed by time - the Eq. (20):

$$\tau_n = \frac{s_n}{c_w} + \frac{s_{no}}{c_b} \quad (20)$$

The pulse response $k(t)$ is determined separately for the path types described above and then added up. For each type, it is the sum of the Dirac pulses, each of which has an amplitude described by Eq. (17), multiplied by the product of the reflection coefficients, which can be described by the Eq. (21):

$$k(t) = \sum_{n=1}^{N} \left[A_n \left(\prod_{k=1}^{n} R_{nk} \right) \delta(t - \tau_n) \right] \quad (21)$$

This is illustrated in the Fig. 7-10 for the sound wave paths of Fig. 2-3, 5-6, which show a reduced number of reflections for clarity. The numbers N of reflections considered while determining pulse responses are given in the figure legends. At the given reflection numbers, there is back propagation, which is discussed in the Part A of the work. The calculations assumed a volume density of water ρ_w = 10^3 kg/m^3, and of bottom sediments ρ_b = 3-10^3 kg/m^3 and logarithmic absorption attenuation coefficients in water α_w = 0.001 dB/m and in bottom sediments α_b = 0.5 dB/m. These were the values occurring at wave frequencies around 5 kHz.

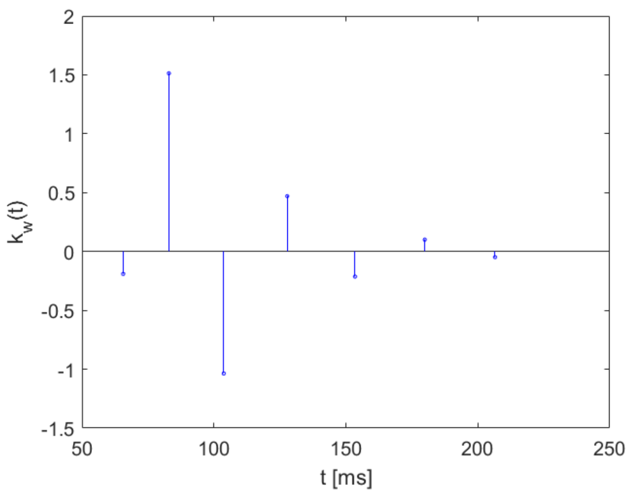

Fig. 7. Pulse response at first reflection from the water surface, $\beta = 3°$, $N = 14$.

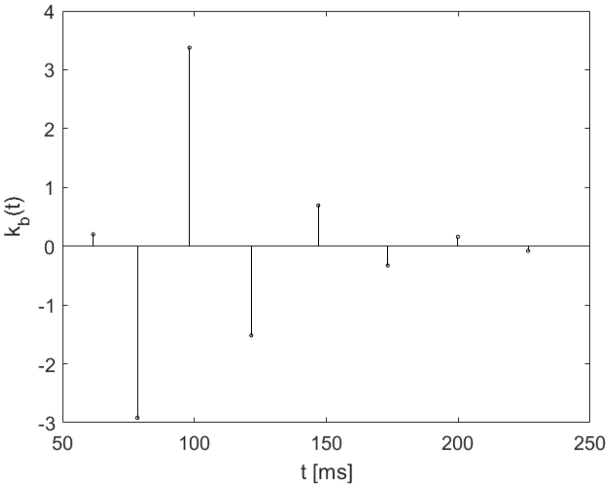

Fig. 8. Pulse response at first reflection from the bottom surface, $\beta = 3°$, $N = 15$.

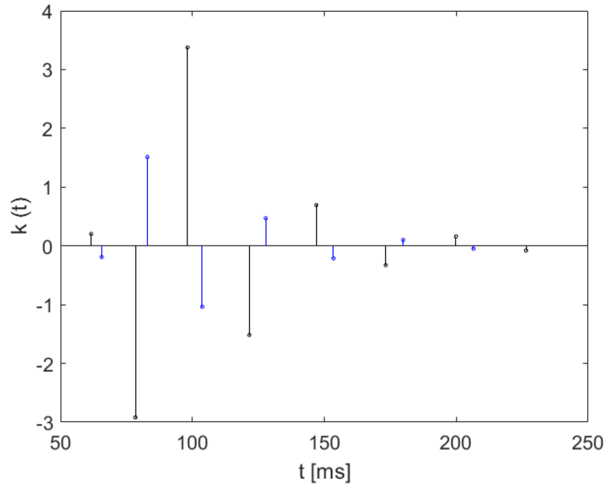

Fig. 9. Total pulse response, $\beta = 3°$.

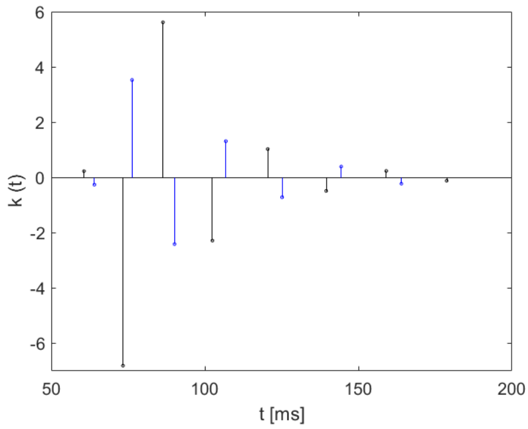

Fig. 10. Total pulse response $\beta = -3°$.

Clear changes can be seen in the pulse response waveforms compared to the response for a communication system with a receiver submerged in water (Part A). The first pulses are much smaller than subsequent pulses, which is a result of the longer propagation in the bottom sediments, in which there is very high absorption attenuation. With a negative slope angle β of the bottom, the response pulses are larger than with a positive angle β. This is reflected in the transfer function waveforms shown in Fig. 11-12.

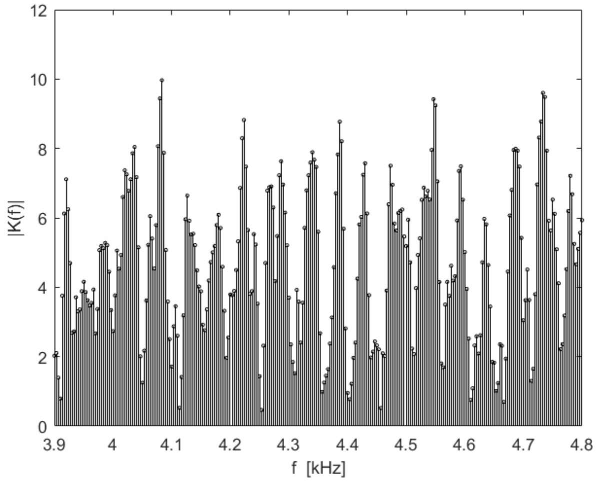

Fig. 11. Transfer function, $\beta = 3°$.

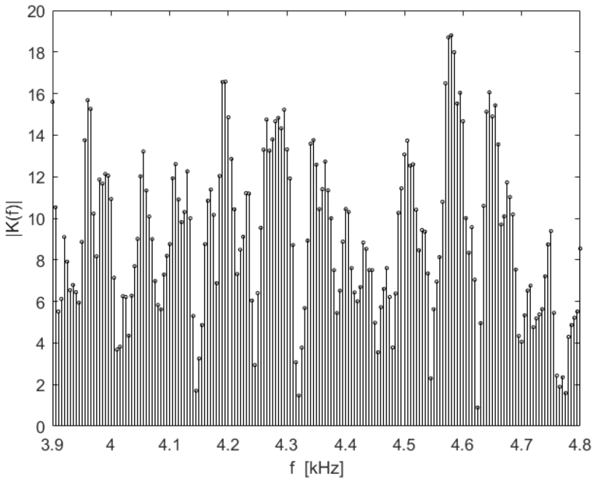

Fig. 12. Transfer function $\beta = -3°$.

IV. Signal transmission

The objective of this work is to investigate the effect of bottom slope on the transmission quality of sound signals. By comparing the transfer functions shown in Fig. 11-12, it can be tentatively concluded that a negative bottom slope is more favorable. A more straightforward answer is provided by examining the transmission of typical signals used in underwater sound communications.

With the determined pulse response of the system of interest, the received signal $x(t)$ is the result of the convolution of the transmitted signal $s(t)$ and the pulse response $k(t)$ described by the Eq. (22):

$$x(t) = k(t) * s(t) \tag{22}$$

Gaussian noise is added to the received signal with a spectral power density N_n. Knowing the magnitude of the received signal $x(t)$ and its spectral width, the input signal-to-noise ratio SNR_i [1] is determined.

Further, the transmission of narrowband pulses and pulsed signals with linear frequency modulation is considered. In the first case, the sum of the signal and noise is filtered in narrowband filters with middle frequencies equal to the carrier frequencies f_0 of the transmitted pulses. The bandwidth of the filters takes into account the Doppler effect and is described by the Eq. (23):

$$B = \frac{1}{\tau} + \frac{v_{max}}{c} f_0 \tag{23}$$

where τ is the pulse duration, v_{max} is the maximum velocity of the transmitter, c is the sound wave velocity in water, and f_0 is the carrier frequency of the pulse.

The received signals are filtered by an eighth-order narrow-band Butterworth filter with a middle frequency f_0 and a bandwidth B. The output signal $z(t)$ is obtained after baseband envelope detection involving rectification of the signal $y(t)$ after filtering, and its low-band processing with a Butterworth filter.

In the case of LFM signals, matched filtering was used, as described by the Eq. (24):

$$y(t) = \mathcal{F}^{-1}\{\mathcal{F}\{k(t)\} \cdot \mathcal{F}^*\{x(t) + n(t)\}\} \tag{24}$$

Where $\mathcal{F}$ denotes the Fourier transform and $*$ is the coupled value.

The output signal z(t) is obtained after baseband envelope detection, as in the case of narrowband pulses.

To illustrate the transmission of narrow-band sinusoidal pulses, two pulses, representing bits ‘0’ and ‘1’, were used, with carrier frequencies f_0 = 4 kHz and f_1 = 4.7 kHz, duration τ = 25 ms at intervals of 4τ = 100 ms. The interval is the assumed duration of the pulse response plus the duration of the pulse. The transmitter is stationary and the filter bandwidth is B = 135 Hz. The transmission is in a channel and system whose pulse response is shown in the Fig. 9. The Fig. 13-16 illustrate signal waveforms at significant points in the system.

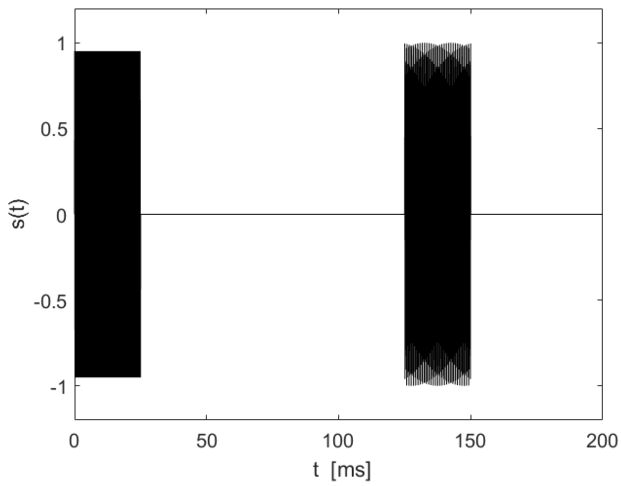

Fig. 13. Signal transmitted.

The figures show that the durations of the output signals mainly depend on the duration of the pulse response and, regardless of the duration of the transmitted pulse, cannot be shorter than this. This necessitates the use of large time intervals between adjacent pulses and thus limits the transmission velocity.

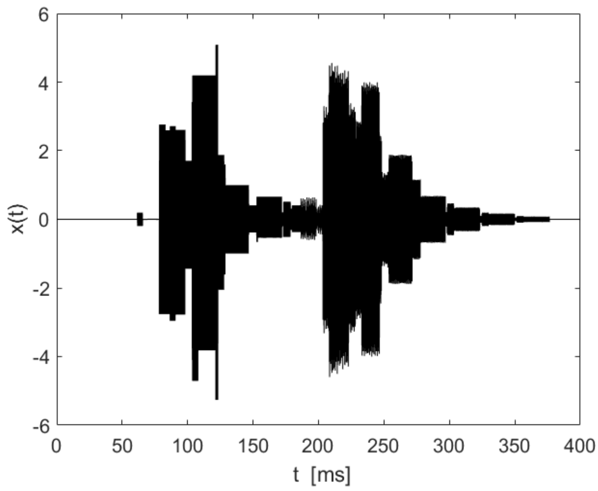

Fig. 14. Receiver input signal.

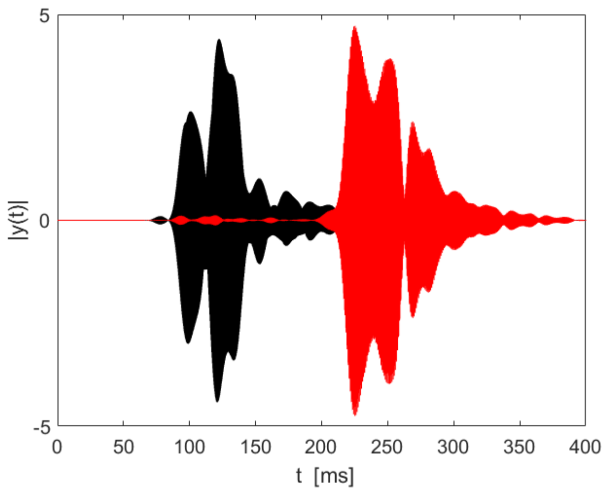

Fig. 15.Signals after narrow-band filtering

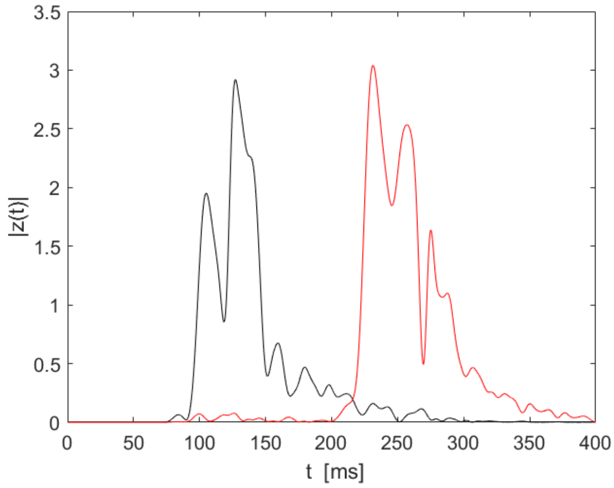

Fig. 16. Baseband envelopes of outputsignals

The output signal waveforms depend strongly on the choice of carrier frequencies, as illustrated by the example shown below, in which the carrier frequency f_1 was shifted by 50 Hz to f_1 = 4,650 Hz. There is a noticeable change in the height of the received pulses, which results from the transfer function shown in the Fig. 11.

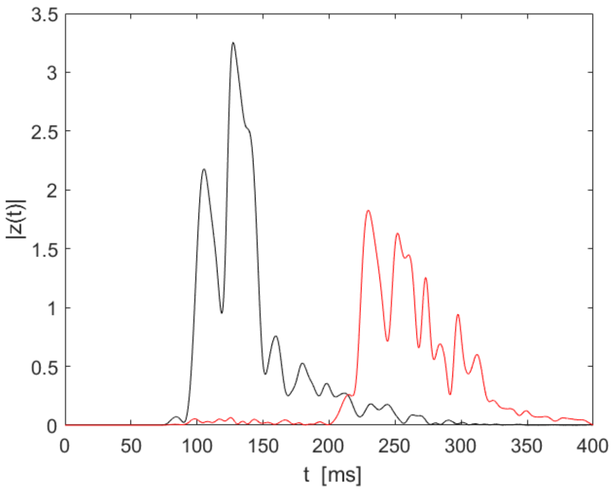

Fig. 16. Baseband envelopes of output signals with shifted carrier frequency.

To investigate the effect of bottom inclination on signal transmission, Gaussian noise with spectral power density N_n was added to the received signal, for three different bottom slope angles β. Noise of higher intensity causes transmission errors. The error percentage *Er* was estimated for 10,000 transmissions by detection each time. It involves comparing the maximum magnitudes of the output signals in the bit reception intervals. If, in the first interval, the signal of bit '1' (black plot line in the figures) is greater than that of bit '0', the transmission is corrected. Otherwise, an error occurs. An analogy was followed for the second interval. The error rate was added up and divided by the number of samples. The calculation results are shown in the Fig. 17. The reason for the differences in error rates is due to differences in the magnitude of the input signal-to-noise ratio SNR_i, as illustrated in the Fig.18.

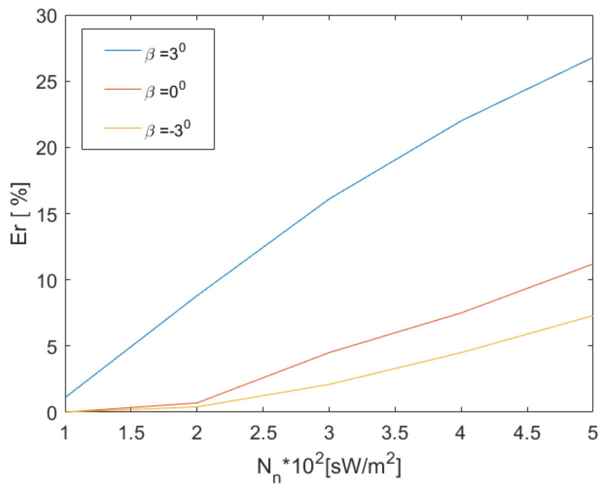

Fig. 17. Transmission error rate for bottom slope angles β.

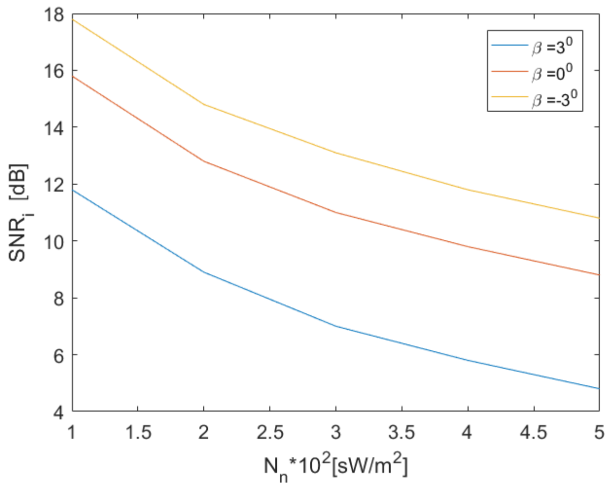

Fig. 18. Input SNR for bottom slope angles β.

From Fig. 16-17 it is evident that the transmission quality increases as the bottom angle β decreases, as confirmed by numerical experiments performed for different channel and system parameters.

The bottom slope also affects the transmission of signals with linear frequency modulation, LFM. It is demonstrated using the example of two pulses with duration $\tau = 0.5$ s, with the carrier frequencies used in the previous calculations and spectral width B = 400 Hz. The pulses are transmitted at a time interval of 0.1 s, as illustrated in the Fig. 19. The magnitude spectrum of the transmitted signals is shown in the Fig. 20.

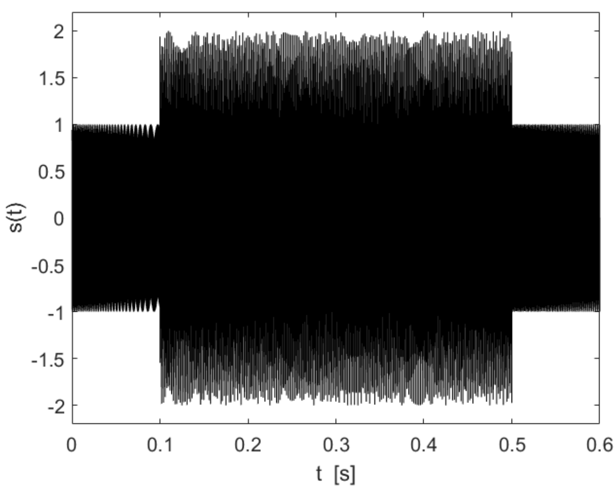

Fig. 19. Transmitted LFM signal.

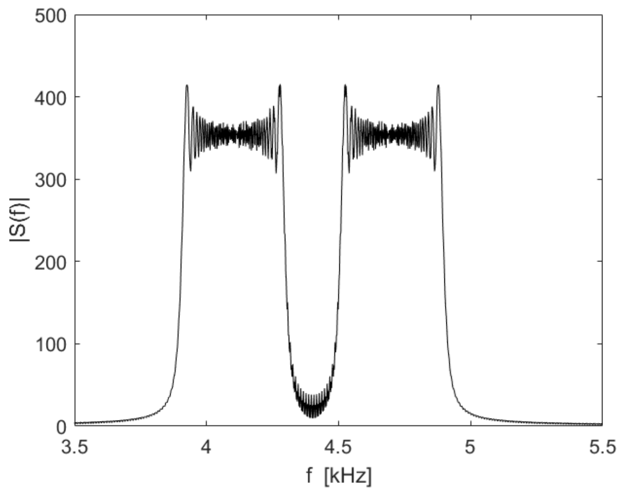

Fig. 20. Transmitted signal spectrum.

The received signal was determined from the Eq. (22), in which the pulse response was derived from the channel and system parameters, carried over from the narrowband pulse transmission example and shown in the Fig. 9. The input signal waveform is illustrated in the Fig. 21. This signal is processed by the matched filtering described by Eq. (24) and the result is shown in the Fig. 22. Filtering is done separately for the two signals representing the '1' and '0' bits, as shown using the different colours.

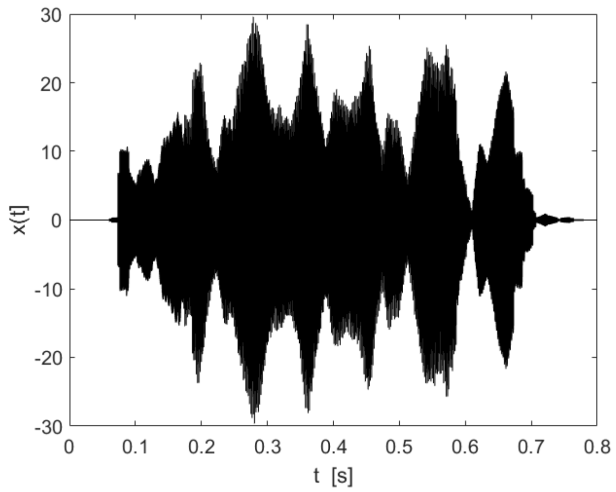

Fig. 21. Received signal

The signals after matched filtering are detected by their rectification and filtering in two 8th order Butterworth filters with bandwidth *B*. These have the waveforms (baseband envelopes) shown in Fig. 23.

It is understood that with ideal filtering matched to the LFM signal, the output signal is a very short pulse of 1/B duration. In the system of interest, it is significantly extended due to the long duration of the pulse response, which requires the long time offset of the transmitted pulses used here. This offset can, however, be smaller than the pulse duration, as shown in the Fig. 24. As a result, transmission speed can be relatively high.

To investigate the effect of bottom slope angle on transmission quality, the numerical experiment described for the case of narrowband pulses was repeated. Examples of the noise output signals are shown in the Fig. 24 and the calculation results are provided in Fig. 25-26.

.

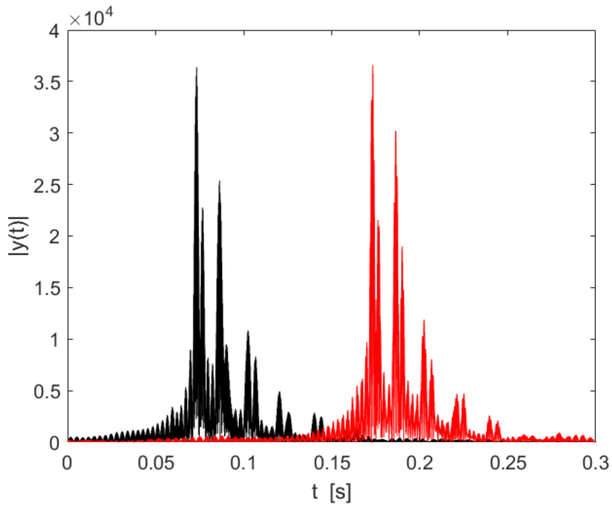

Fig. 22. Signals after matched filtering.

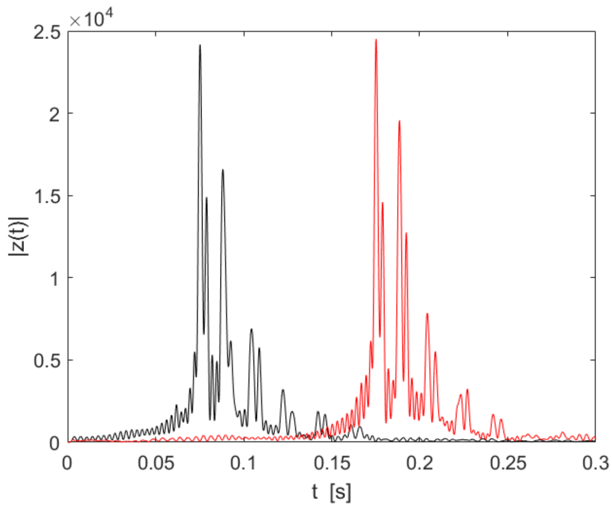

Fig. 23. Noise-free baseband envelopes of output signals: bit '1' – black plot line; bit '0' – red plot line.

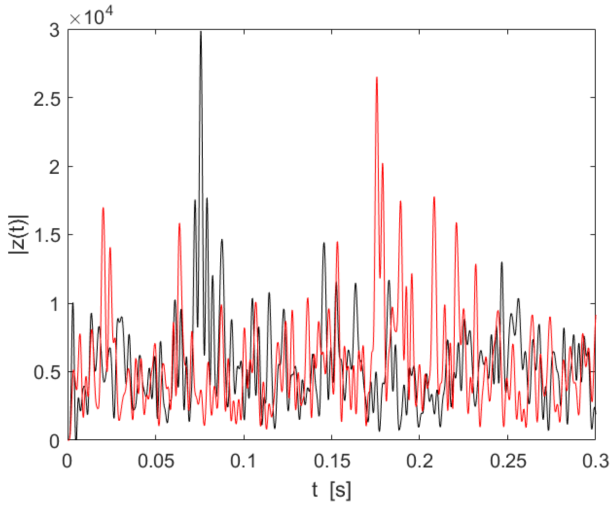

Fig. 24. Noisy baseband envelopes of.output signals

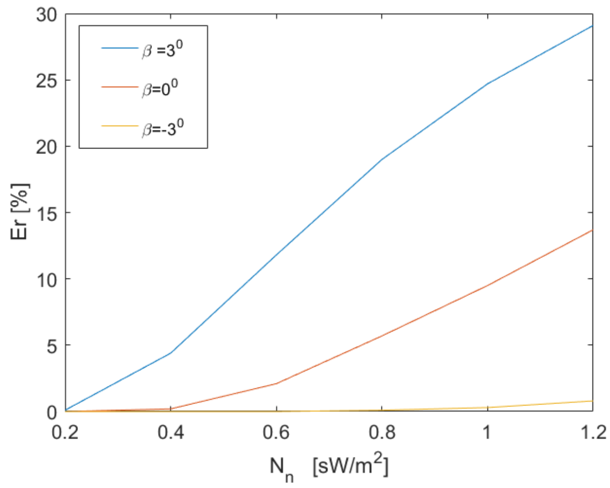

Fig. 25. Transmission error rate for bottom slope angles β.

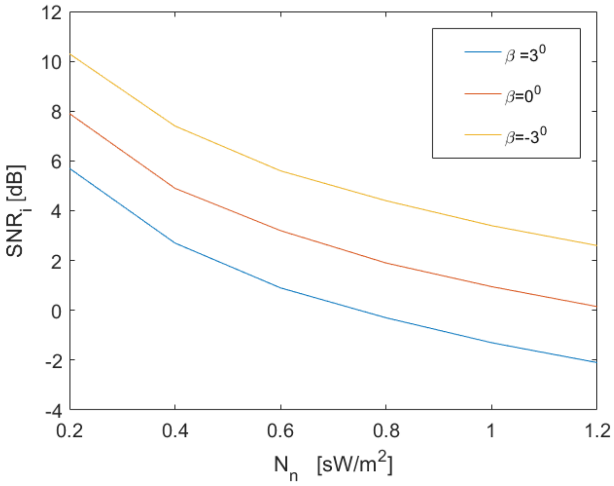

Fig. 26. Input SNR for bottom slope angles β.

The Fig. 25 confirms the previously noted trend of better transmission quality for smaller bottom slope angles. The use of LFM signals provides much better detection conditions than narrowband pulsed signals, as a comparable transmission error rate is achieved with a lower noise level described here by the spectral power density N_n. For example, in the Fig. 17, for the bottom slope angle β = 3°, similar error rates to those shown in the Fig. 25 are achieved with N_n approximately 500 times lower. This is due to the improvement of the output SNR_o to the input SNR_i for signals with LFM. The input SNR levels shown in Fures 18 and 26 are similar.

Conclusions

This work showed that there is a significant effect of the bottom slope angle on the quality of sound signal transmission from a transmitter submerged in the water to a receiver buried in the bottom sediments. The improvement in detection conditions is greater the smaller the slope angle, and especially when this angle is negative. An analogous trend occurs for transmissions between a transmitter and receiver immersed in water, as demonstrated in the Part A of the work. As in this work, the benefits of using linear frequency modulated signals in an underwater communication system are shown.

It can be assumed that the trend shown occurs in real systems with wave dispersion on the water surface and bottom, the impact of which was not considered in the article. As a result of scattering, the wave is reduced in size, however, the greater part of it travels along a path satisfying the mirror reflection conditions adopted for simplicity of analysis.

Notice

In the paper – “Part A”, these authors demonstrate the effect of bottom slope on transmission with the receiver submerged in water column

References

[1] R. Salamon, J. Marszal, I. Kochańska., “Shallow Water Communication with an Object Buried in Bottom Sediments”, Intl Journal of Electronics and Telecommunications, 2024, Vol. 70, No. 4, pp. 805-813. doi: 10.24425/ijet.2024.152064

[2] I. Kochańska, A. M. Schmidt, JH. Schmidt, “Shallow-Water Acoustic Communications in Strong Multipath Propagation Conditions”, *2024 14th International Symposium on Communication Systems, Networks and Digital Signal Processing (CSNDSP)*, IEEE *Xplore*, pp. 99-103, 2024. doi: 10.1109/CSNDSP60683.2024.10636410

[3] J. H. Schmidt, A. M. Schmidt, I. Kochańska, R. Studański, A. Żak, “Performance of underwater data transmission using incoherent modulation MFSK in very shallow waters”, *International Journal of Electronics and Telecommunications,* vol. 70, no.4, pp. 861-869, 2024. doi: 10.24425/ijet.2024.152071

[4] J. H. Schmidt, I. Kochańska, A. M. Schmidt,“Performance of the Direct Sequence Spread Spectrum Underwater Acoustic Communication System with Differential Detection in Strong Multipath Propagation Conditions”, *Archives of Acoustics,* vol. 49, no. 1, pp. 129-140. doi: 10.24425/aoa.2024.148771

[5] J. Schmidt, I. Kochańska, A. Schmidt, “Measurement of impulse response of shallow water communication channel by correlation method”, *Hydroacoustics*, vol. 20, pp. 149-158, 2017.

[6] I. Kochańska, J. H. Schmidt, J. Marszal, “Shallow water experiment of OFDM underwater acoustic communications”, *Archives of Acoustics*, vol. 45, no. 1, 11-18, 2020, doi: 10.24425/aoa.2019.129737

[7] J. B. Allen, D. A. Berkley, “Image method for efficiently simulating small-room acoustics”. *J. Acoust. Soc. Am.*, vol. 65, no. 4, pp. 943-950, 1979. doi: 10.1121/1.382599

[8] A. Wareing, M. Hodgson, “Beam-tracing model for predicting sound fields in rooms with multilayer bounding surfaces, *J. Acoust. Soc. Am.*, vol. 118, no. 4, pp. 2321-2331, 2005. doi: 10.1121/1.2011152

[9] G. Marbjerg, J. Brunskog, C. H. Jeong, E. Nilsson, “Development and validation of a combined phased acoustical radiosity and image source model for predicting sound fields in rooms”. *J. Acoust. Soc. Am.*, vol. 138, no.3, pp. 1457-1468, 2015. doi: 10.1121/1.4928297

[10] M. Stojanovic, J. Preisig, “Underwater acoustic communication channels: prpagation models and statistical characterisation”, *IEEE Communications Magazine*, January 2009, pp. 84-89, 2009. doi: 10.1109/MCOM.2009.4752682

[11] T. C. Yang, “Properties of underwater acoustic communication channels in shallow water”, *J. Acoust. Soc. Am.*, vol. 131, no. 1, pp. 129-145, 2012. doi: 10.1121/1.3664053

[12] P. A. van Walree, “Propagation and scattering effects in underwater acoustic communication channels”, *IEEE J. Ocean Eng.*, vol. 38, no. 4, pp. 614-631, 2013.

[13] F. John, M. Cimdins, H. Hellbrück, “Underwater ultrasonic multipath diffraction model for short range communication and sensing applications”, *IEEE Sensors Journal*, vol. 21, no. 20, pp. 22934-22943, 2021.